



Carbon fiber/carbon nanotube reinforced hierarchical composites: Effect of CNT distribution on shearing strength



H.W. Zhou ^{a, *}, L. Mishnaevsky Jr. ^{b, **}, H.Y. Yi ^a, Y.Q. Liu ^a, X. Hu ^a, A. Warrier ^{c, 1}, G.M. Dai ^b

^a State Key Laboratory of Coal Resources and Safe Mining, China University of Mining and Technology, Beijing 100083, China

^b Technical University of Denmark, Department of Wind Energy, Risø Campus, DK-4000 Roskilde, Denmark

^c KU Leuven, MTM, B-3001 Heverlee, Belgium

ARTICLE INFO

Article history:

Received 7 June 2015

Received in revised form

15 October 2015

Accepted 21 October 2015

Available online 14 November 2015

Keywords:

A: Polymer-matrix composites (PMCs)

A: Nano-structures

B: Fracture

C: Finite element analysis (FEA)

D: Mechanical testing

ABSTRACT

The strength and fracture behavior of carbon fiber reinforced polymer composites with carbon nanotube (CNT) secondary reinforcement are investigated experimentally and numerically. Short Beam Shearing tests have been carried out, with SEM observations of the damage evolution in the composites. 3D multiscale computational (FE) models of the carbon/polymer composite with varied CNT distributions have been developed and employed to study the effect of the secondary CNT reinforcement, its distribution and content on the strength and fracture behavior of the composites. It is shown that adding secondary CNT nanoreinforcement into the matrix and/or the sizing of carbon fiber/reinforced composites ensures strong increase of the composite strength. The effect of secondary CNTs reinforcement is strongest when some small addition of CNTs in the polymer matrix is complemented by the fiber sizing with high content of CNTs.

© 2015 Elsevier Ltd. All rights reserved.

1. Introduction

The development and use of lightweight, strong, damage resistant materials determine the progress and efficiency of many industrial areas, among them, in aerospace, automobile, defense, sports and energy. For instance, perspectives of renewable energy development depend on the development and use of highly reliable, extra-large wind turbines, working reliably over several decades with minimum maintenance and repair [1] and need therefore correspondingly strong materials.

A number of experimental and computational investigations have been devoted to the development of such materials [1–20]. While most widely used polymer composites now are based on glass fiber reinforcement, carbon fibers composites are attracting a growing interest of research community and industry, due to their high to density ration, high strength and stiffness. Replacement of the glass fiber reinforcement by carbon fibers allows reducing the weight and improvement of the tensile strength and stiffness of the

composites [1–5]. On the other side, carbon fibers demonstrate relatively low compressive strength, and are much more expensive than glass fibers [5]. Another path of the improvement of the composite properties, which also is attracting a large interest of researchers and industry recently, and which is based on introducing the secondary nanoscale reinforcement (e.g., graphene, carbon nanotubes or nanoclay distributed in polymer matrix or fiber sizing) into the fiber reinforced composites [6]. Some literature show that the addition of a small amount of nanoparticles into the matrix or fiber sizing of fiber reinforced composites can be used to improve composite properties, first of all, matrix-dominated properties (flexural and interlaminar shear and compressive strength and fatigue resistance of composites) [7–20]. In several works, the positive effect of nanoreinforcement on the interlaminar strength of composites has been observed [8,9,12]. So, the deposition of multi and single walled CNT on woven carbon fabric fibers in epoxy matrix led to 30% enhancement of the interlaminar shear strength [8,9]. Interlaminar toughness and strength of alumina fiber reinforced plastic laminates are improved by 76% due to the radially aligned CNTs in both interlaminar and intralaminar regions [11]. Storck et al. [12] studied experimentally the effect of CNTs on mode I interlaminar strength, and observed that high densities of short nanotubes can lead to the improvement of interlaminar strength up to 29% (in glass fiber composites).

* Corresponding author. Tel.: +86 1062331286; fax: +86 10 62331490.

** Corresponding author. Tel.: +45 46775729; fax: +45 46775758.

E-mail addresses: zhw@cumtb.edu.cn (H.W. Zhou), lemi@dtu.dk (L. Mishnaevsky).

¹ Current address: Blades Technology B.V., 7559 ST Hengelo, The Netherlands.

Warrier et al. [13] studied the mode-I interlaminar fracture toughness of glass fiber reinforced composite integrated with CNTs in fiber sizing, matrix and both, CNTs in the three phases increased the fracture toughness while CNTs in matrix or fiber sizing shows decrease of crack propagation toughness. In Refs. [14,15], the authors observed that the crack initiation toughness increases when CNTs were introduced into carbon fiber/epoxy composites (by 10% if CNTs in sizing and by 25% if in matrix) [16]. Zhou et al. [17] demonstrated that 2 wt% carbon nano-fibers in matrix improved the interlaminar shear strength (ILSS) by 22.3%. The coating on the glass fibers with single-wall CNTs increased the ILSS of composites by 35% [18,19]. Gojny et al. [20] showed that multiple-wall CNTs in the matrix enhanced the ILSS of composites. Through the contribution of CNTs to the fiber bridging and interfacial strength, the CNTs in the matrix lead to the improvement of the fracture toughness of composites. Adding the CNTs in fiber sizing leads to the creation of tough and stiff region around fibers thus improving the interfacial shear strength of composites [16].

While the high potential of carbon fiber reinforced composites with secondary nanoreinforcement have been demonstrated in many works, the question arises how the nanoparticles content, distribution, localization and orientation influence the strength of the composites. In this paper, experimental and computational investigations of strength and damage mechanisms of carbon fiber reinforced polymer composites with secondary CNT nanoreinforcement were presented. The effect of the availability and distribution of CNTs (in fiber sizing and in matrix) was studied, in terms of the damage mechanisms, intralaminar and interlaminar fracture strength of the composites.

2. Materials and testing methodology

2.1. Materials and samples

In order to investigate the effect of secondary nanoreinforcement on the damage and failure behavior of hierarchical composites, a series of experimental investigations was carried out. Six types of samples had been fabricated and tested: carbon fiber/epoxy composites with and without CNTs in matrix, with and without CNTs in the fiber sizing, with varied content of CNTs in the fiber sizing, as well as with virgin matrix and sizing (Table 1). The following components of the composites were used for the fabrication of samples:

2.1.1. Matrix

An epoxy resin based on diglycidylether of bisphenol A (DGEBA) formulated for hotmelt prepreg processing with hardener Aradur-5021 was used as a matrix. The glass transition temperature of the neat resin was around 110 °C, density ~ 1.18 g/cc, CTE 66×10^{-6} /°C, Young modulus 2.7 GPa. The epoxy matrix without nanotubes is referred below as EP.

2.1.2. Carbon nanotubes and modification of matrix

Multiwalled carbon nanotubes (MWCNTs) were produced and supplied by Nanocyl (Belgium) – (Nanocyl[®]-7000 series). The nanotubes have average diameter of 9.5 nm, Average length: 1.5 micros (obtained from SEM/TEM analysis), specific surface of 250–300 m²/g and carbon purity >90%. The MWCNTs were dispersed in the epoxy resin, with the concentration 0.5 wt%. The homogenous dispersion was achieved using calendaring equipment consisting of three rolls which generate high-shearing forces by controlling the spacing between them and their speed. The epoxy matrix with nanotubes is referred below as EPNT.

2.1.3. Carbon fibers and their sizing

The carbon fibers (Toho Tenex) were directly coated with MWCNTs size by Nanocyl (Belgium) without removal of the commercial sizing. The coating was done by drawing the fibers through water soluble, epoxy-compatible phenoxy-based sizing having varied weight percentage of MWCNTs and subsequent drying at 120 °C. The properties of commercial carbon fibers are as follows: Toho Tenex (Grade 12 K, Tex-800) Density (gm/cc) 1.76 Diameter (μ m) 10, Tensile strength 3920 MPa, Tensile modulus 234 MPa, failure strain 1.7%. The descriptions of modified fibers are shown in Table 2. Fig. 1 shows SEM images of modified carbon fibers.

2.1.4. Fabrication of composites

The CNT-fiber reinforced unidirectional (UD) composites were produced using a drum winder. Once the prepregs were prepared, they were stored in a refrigerator at temperature ~ -18 °C. Finally, UD composite plates were produced. The prepregs were cut into sheets with dimensions 300 mm by 300 mm. To produce a composite plate, eight such prepregs were laid up in unidirectional fiber orientation and were cured at 120° for 60 min followed by a post curing step at 140 °C for 120 min. The laminates were produced in an autoclave at vacuum of -0.65 to -0.70 bar, in a vacuum bag using peel-ply and bleeder. Flow of the resin was consistently seen in the bleeder. The amount of the bled resin depends upon the viscosity of the resin system (epoxy or epoxy with CNTs). Composite laminates with a thickness of about 2.5–3.5 mm were obtained with the final fiber volume fraction in the range from 50 to 55% (ASTM D3171). Fig. 2 shows the scheme of composite preparation with the prepreg technique.

2.2. Specimen preparation

Water jet technology (OMAX-2626xP/30HP Jet Machining), available at Chongqing University was employed to cut composite plates into cuboids' shape. Widths of margins of each cutting edge were set as 2 mm. The dimensions of specimen are given in Table 3. Polished specimen were cleaned in alcohol by ultrasonic clearing machine for 5 min, then gilt by ion sputter for 200 s (gilding layer would be approximately 11 nm in thickness which does nearly no

Table 1
Specimens and their components.

Identification code	Sample code	Materials description
85/EP	CF0/EP-n	No MWNTs in fiber sizing and pure matrix
85/EPNT	CF0/EPNT-n	No MWNTs in fiber sizing and 0.5 wt% MWNTs in matrix
87/EP	CF50/EP-n	50% MWNTs in fiber sizing and pure matrix
87/EPNT	CF50/EPNT-n	50% MWNTs in fiber sizing and 0.5 wt% MWNTs in matrix
86/EP	CF25/EP-n	25% MWNTs in fiber sizing and pure matrix
86/EPNT	CF25/EPNT-n	25% MWNTs in fiber sizing and 0.5 wt% MWNTs in matrix

Table 2
Description of modified carbon fibers.

Identification code	Batch number	Materials description
85	FL-C7200/1585	1 Kg of 800 tex Carbon fibers were coated with 0.5% nominal solids with pure sizing (no MWNTs)
87	FL-C7200/1587	1.05 Kg of 800 tex Carbon fibers coated with 0.5% nominal solids with sizing containing MWNTs (50:50)
86	FL-C7200/1586	0.94 Kg of 800 tex Carbon fibers coated with 0.5% nominal solids with sizing containing MWNTs (25:75)

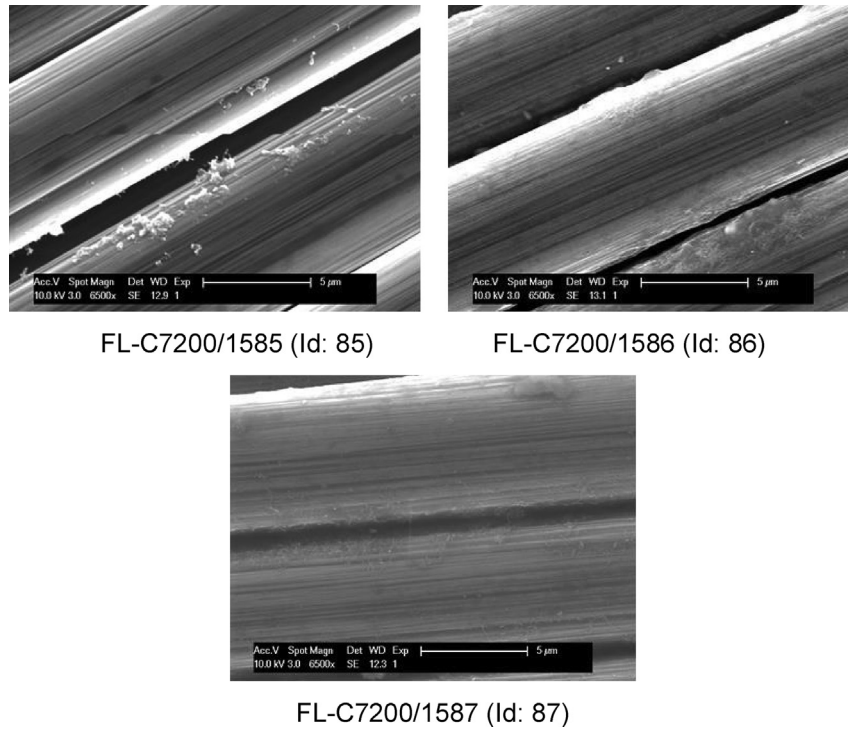


Fig. 1. SEM images of carbon fibers with MWNTs size.

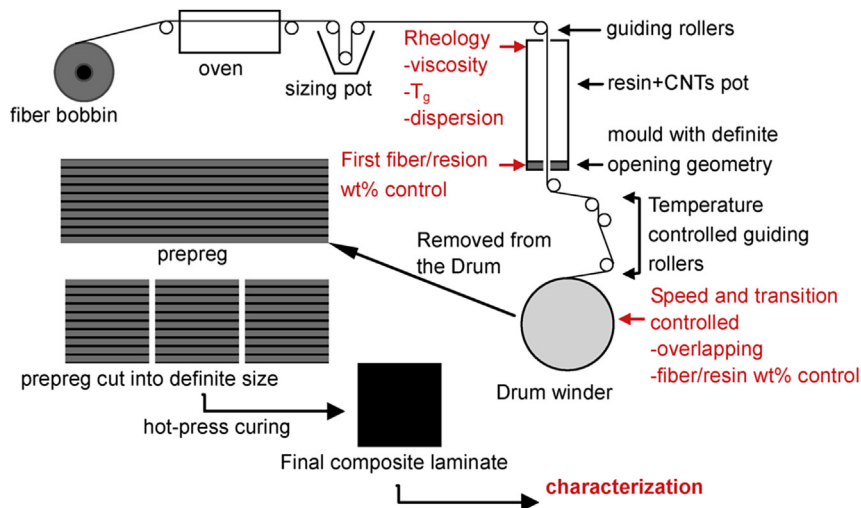


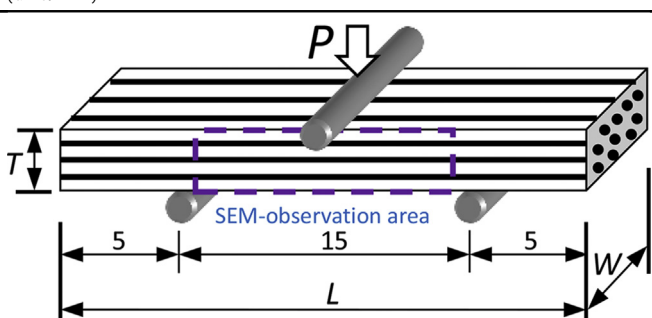
Fig. 2. Schematic view of composite preparation.

effect on observation of micro-structure) after the alcohol was evaporated completely. All the specimens were divided into 6 categories with respect to the dispersing location and volume fraction of CNTs. 6 specimens were prepared for each category, 36 specimens totally.

2.3. Short beam shearing tests

Short Beam Shearing (SBS) tests were carried out corresponding to the ASTM-D2344 standard [21]. The SEM fatigue testing system available at China University of Mining and Technology in Beijing

Table 3
Dimensions of specimen.

Specimen code	Specimen dimensions (unit: mm)	Length <i>L</i> /mm	Width <i>W</i> /mm	Thickness <i>T</i> /mm
CF0/EP		25 ± 1	6 ± 0.3	3.6 ± 0.1
CF0/EPNT		25 ± 1	6 ± 0.3	4.1 ± 0.1
CF50/EP		25 ± 1	6 ± 0.3	2.3 ± 0.08
CF50/EPNT		25 ± 1	6 ± 0.3	4.4 ± 0.06
CF25/EP		25 ± 1	6 ± 0.3	2.7 ± 0.1
CF25/EPNT		25 ± 1	6 ± 0.3	3.5 ± 0.1

(developed and provided by Shimadzu Co., Japan) was used in the experiments (see more details in Refs. [22–24]). This system consists of loading device, SEM and data collection device. Full digital servo hydraulic control allows loading up to ±10 kN and load frequency of 1×10^{-5} –10 Hz. SEM employed during the loading process allows observing micro-structural change of specimen, and data collection device helps displaying load–displacement of the whole loading process. Displacement controlled loading with a speed of 2×10^{-3} mm/s was applied to the specimens. The load–deflection data and curves were recorded by the SEM automatically. During the loading process, the in-situ SEM pictures were taken.

The Interlaminar Shearing Stress (ILSS) were calculated by $ILSS = \frac{3P_n}{4bt}$, where P_n means maximum load, b and t represent width and thickness of specimen, respectively. It should be noted that this value is defined as interlaminar shearing stress only assuming that the specimen fails by interlaminar cracking indeed. If more or other mechanisms participate, this value still characterizes the material strength, but only in more general case.

3. Failure mechanisms in hierarchical carbon/CNT composites: experimental investigations

3.1. Deformation behavior of the composites

Fig. 3 shows the force–deflection curves obtained in the experiments. The specimen without CNTs in matrix (Fig. 3a, c, e) underwent an initial cracking when their load–deflection curve arrived at the near-peak points, then their load–deflection curve begins to fluctuate and decreases gradually. Initial cracking of specimen with certain volume fraction of CNTs in the matrix (Fig. 3b, d, f) has been observed when the load–deflection curve reached nonlinear region, which is longer than that for the specimen without CNTs in matrix.

In the composites with high content of CNTs in fiber sizing (50%) (Fig. 3b, d), the shear stress remained quite high even after load–deflection curve went the peak points. For the composites with lower fraction of CNTs (25%), this effect was not observed. This demonstrates that the CNTs in the fiber sizing play a positive role of increasing the delaminating resistance of CFRP, however, the fraction of CNT should be rather high. This corresponds to the results by Storck et al. [12] who observed that especially high densities of CNTs grown on fibers leads to the drastic improvement of interlaminar strength of composites.

Fig. 3 also shows that the initial delamination took place in all specimens before their load–deflection curves reach the peak

points. In order to compare and obtain the ILSS, the normalized interlaminar shear stress were calculated based on the equation of ILSS according to ASTM-D2344. The normalized interlaminar shear stress–deflection curves are shown in Fig. 4a. Fig. 4b gives the average interlaminar strengths for the considered composites. From Fig. 4a and b, it can be seen that the specimens with CNTs distributed in the matrix (CF0-EPNT and CF50-EPNT) have the highest ILSS, while the specimens without CNTs at all (CF0-EP) show the lowest ILSS values.

Comparing the ILSS values, one can conclude that the addition of CNTs in the matrix leads to the increase of ILSS by 77% (without any modifications of sizing). The addition of CNT in the fiber sizing (keeping matrix CNT free) increases the toughness by 36%–53%. The addition of both CNTs in fiber sizing and in matrix leads to the increase in the ILSS by 42%–88%. The strong role of CNTs in matrix is related with the fact that the failure mechanism is controlled by interlaminar cracking (i.e., strongly matrix controlled). Thus, one can conclude that adding secondary CNT reinforcement in the composite leads to the increase of the fracture resistance of composites.

The observations correspond to results reported in the literature. So, Wicks and colleagues also observed the increased interlaminar toughness and strength of alumina fiber reinforced plastic laminates (by 76% and 9%, respectively) due to the CNTs in interlaminar and intra-laminar regions [11]. Wichmann et al. [50] reported 16% improvement of interlaminar shear strength by adding 0.3 wt% CNTs to the matrix of glass composites.

3.2. Failure process and mechanisms

Figs. 5 and 6 show the micrographs of the damaged and cracked specimen. In the specimens with the virgin matrix, the peak stress and the end of linear deformation stage corresponded to the point of the initial delamination of the composite (Fig. 5a–c). The stress–strain curves went down after the delamination crack formed. With increasing deformation, the delaminating crack did not propagate further, but turned into the delaminated layers fractured at the crack tips. The stress–strain curve fluctuated and went down after the formation of new delamination cracks and the layer breakage.

Specimen with nano-reinforced matrix (Fig. 5d, e) did not show apparent damage in the early stages of nonlinear deformation. Only, after the initial delamination, the slope of the load–deflection curves becomes negative while the load still increases. The interlaminar crack propagation led to the slight decrease in load–

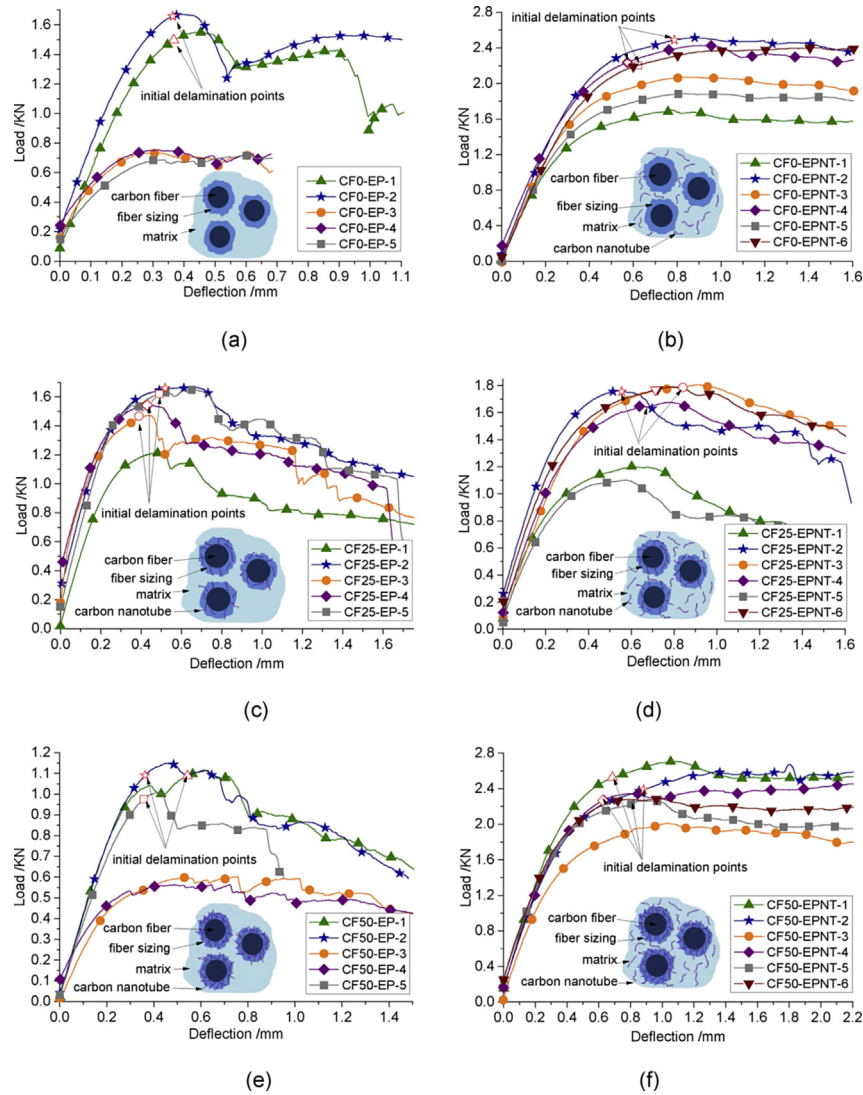


Fig. 3. Load–deflection curve of specimen (a) CF0-EP, (b) CF0-EPNT, (c) CF25-EP, (d) CF25-EPNT, (e) CF50-EP, (f) CF50-EPNT.

deflection curves (except for the specimen CF25-EPNT), while the stiffness of the material still remained high.

In the specimens CF0-EP, CF0-EPNT and CF50-EPNT, cracks forming in the fiber/matrix interfaces and developing parallel to the layers have been observed inside the plies. In the specimen CF50-EP, only interlaminar crack propagation was observed. In the specimen CF25-EPNT, both cracks inside the plies (intralaminar cracking) and interlaminar crack just near the intralaminar crack was observed. In the specimen CF50-EP, the delaminating area could not be identified. Further, specimens with CNTs in matrix (Fig. 5d–f) have more delaminated layers than the corresponding specimen without CNTs in matrix (Fig. 4a–c), while they underwent less layer fracture during the loading process. Fig. 5a–c shows that delaminated layers in the specimens without CNTs in the matrix failed immediately after the load–deflection curves surpass the peak load. The broken plies show compressive patterns.

Comparing the detailed SEM pictures of specimens with virgin matrix (Fig. 6a–c), and with virgin fiber sizing CF0-EP, one can see that the cracks in the broken plies run across the middle area of specimen. The fibers in the delaminated layer have smooth surface. The delaminating crack in CF0-EPNT propagated along the fibers/sizing interface.

When the fiber sizing contains 25% of CNTs (CF25-EP and Fig. 6c), fiber pull-out took place during the shearing process. The fiber surface is rough, contains fractured fiber sizing while the fiber sizing around the broken fibers was debonded to some extent. Apparently, a crack propagated along the sizing/matrix interface, also, through the fiber sizing, then which lead to fiber pull-out or shear fracture. From the SEM micrographs (Fig. 6d–f), one can see that the plies were cracked after the delaminating cracks propagated to some extent. In the specimens with 25% CNTs in fiber sizing, the plies were broken in middle area of specimens and delaminating crack propagated through the layers.

When the fiber sizing contains 50% of CNTs (CF50-EP), the fracture surface along the fibers is quite rough, and some matrix parts still adhered to the fiber surface after delamination. Thus, the crack initiated in the matrix propagated along the fibers or sizing/matrix interface, along a quite zigzagged path controlled by the CNTs.

It is of interest to compare these results with some literature data. Zhang et al. [51] and Sager et al. [52] tested carbon/CNT/epoxy hierarchical composites with various sizings and orientations of MWCNT, and observed that randomly oriented CNT and aligned CNT ensure 71% and 11% increase of interfacial shear strength as compared with unsized fibers. In Refs. [14,15], the authors compared

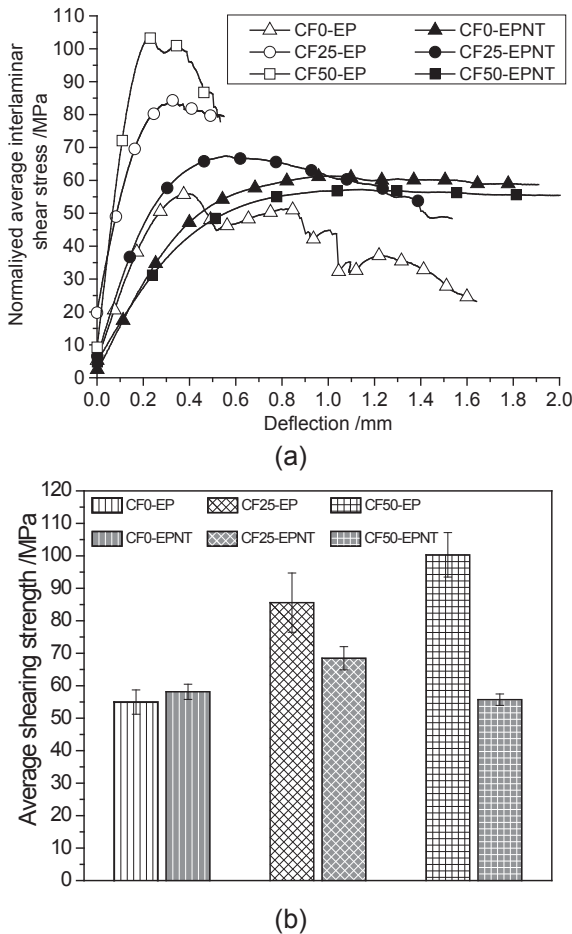


Fig. 4. Normalized interlaminar shear stress–deflection curve (a) and average interlaminar shear strength (balk diagram) (b).

the composites with CNTs dispersed in matrix and distributed in fiber sizing. They observed that the crack initiation toughness increases by 10% if CNTs in sizing and by 25% if in matrix [16].

One can conclude that the nanoreinforcement in the matrix changes the mechanism of degradation of laminates. The matrix (also interlaminar) fracture and the fiber/matrix interface debonding can be considered as competing processes. Adding CNTs into fiber sizing leads to the improvement of the fiber/polymer bonding strength. In the case when the fiber sizing contains relatively high volume of CNTs (while the matrix is not nano-reinforced), the fiber/matrix debonding is delayed/stopped, thus, making the matrix the weakest element in the system. So, only the delamination/cracking between the plies takes place. In the case of nanoreinforced matrix, rather intralaminar cracking takes place.

4. 3D computational modeling of carbon/CNT composites

In this section, 3D computational studies of the damage and fracture in the CNT reinforced carbon fiber composites were carried out and compared with the experimental results.

4.1. 3D multiscale unit cell model

With view on the large difference of the dimension scale of the fiber reinforced composite (macro-scale) and CNTs reinforcement (nano-scale), the concept of macro-micro multiple-step modeling was used here [25], to simulate the damage evolution in the

material. A number of 3D computational unit cell models reflecting the composite structures should be generated. For this, a special Python based software code for the automatic generation of unit cells with multiple cylinder-like reinforcements [25–31] was generalized and improved. The newly developed code allows to generate hierarchical FE models with pre-defined structures, including the macro-scale unit cell (with unidirectional/misaligned fibers and variable fiber content) and lower scale unit cell model (with aligned/random oriented carbon nanotubes, surrounded by the effective interface layers, see Refs. [30,31]), automatically. A hierarchical computational (finite element) model of the composite CF50/EP with CNTs in fiber sizing (50%) is shown in Fig. 7a.

4.2. Damage analysis implementation

The damage and fracture model was developed following [25,26,29]. The procedure of numerical simulation of damage evolution in nanocomposites includes two steps: damage onset and damage propagation [25,32]. The initial defects are introduced by subjecting the unit cell to a quasi-static load. The onset of a crack in a graphene reinforced composite is governed by the maximum principal stress criterion, which can be defined as $f = \{(\sigma_{\max})/\sigma_{\max}^0\}$ [33]. Here, f denotes the maximum principal stress ratio and the damage crack will be formed when $f=1$. σ_{\max}^0 stands for the maximum allowable principle stress and the symbol $\langle \rangle$ is Macaulay brackets which lets the σ_{\max} has the alternative value of 0 or m_{ix} when $m_{ix} < 0$ or $\sigma_{\max} \geq 0$, respectively.

To model the crack propagation, 3D power law $(G_I/G_{Ic})^\alpha + (G_{II}/G_{IIc})^\beta + (G_{III}/G_{IIIc})^\gamma \geq 1$ was used [34]. Here, the symbol G_c denotes the strain energy release rate parameters and indices I, II, III stand for the three fracture modes. The index c represents the critical values of strain energy release rate (the fracture toughness). α, β, γ are parameters and are assigned the value of 1.

The numerical simulation works are carried out with the commercial FE code ABAQUS/STANDARD (version 6.11). The three-dimensional 4-node linear tetrahedron element C3D4 is used for meshing. The virtual crack closure technique (VCCT) [35,36] is used to calculate the strain energy release rate and the linear elastic fracture mechanics (LEFM) approach and the framework of extended-FEM (xFEM) method [37,38] are involved to implement the crack evolution analysis.

4.3. Material properties

The materials and component properties are summarized in Table 4. For the strain energy release rate for fibers, we used the formulation by Pinho et al. [45]:

$$G_{Ic}|_{\text{fiber}} = 2G_{Ic}|_{\text{laminare}} - G_{Ic}|_{\text{matrix intra}} \quad (1)$$

here, $G_{Ic}|_{\text{fiber}}$, $G_{Ic}|_{\text{laminare}}$ and $G_{Ic}|_{\text{matrix intra}}$ stands for the critical strain energy release rate for fiber, the fiber reinforced laminate and the matrix, respectively. When choosing the micro- and nanoscale input data, we sought to use the same values as in our previous works, to make results comparable.

4.4. Computational experiments: effect of CNT distribution on damage and fracture of CNT/carbon fiber composites

In this section, results of the computational studies of the effect of CNT distribution on the damage and strength of hierarchical CNT/carbon composites are presented.

Fig. 7b shows the calculated shear stress–strain curves. It can be seen that the obtained strengths of the composites differ from

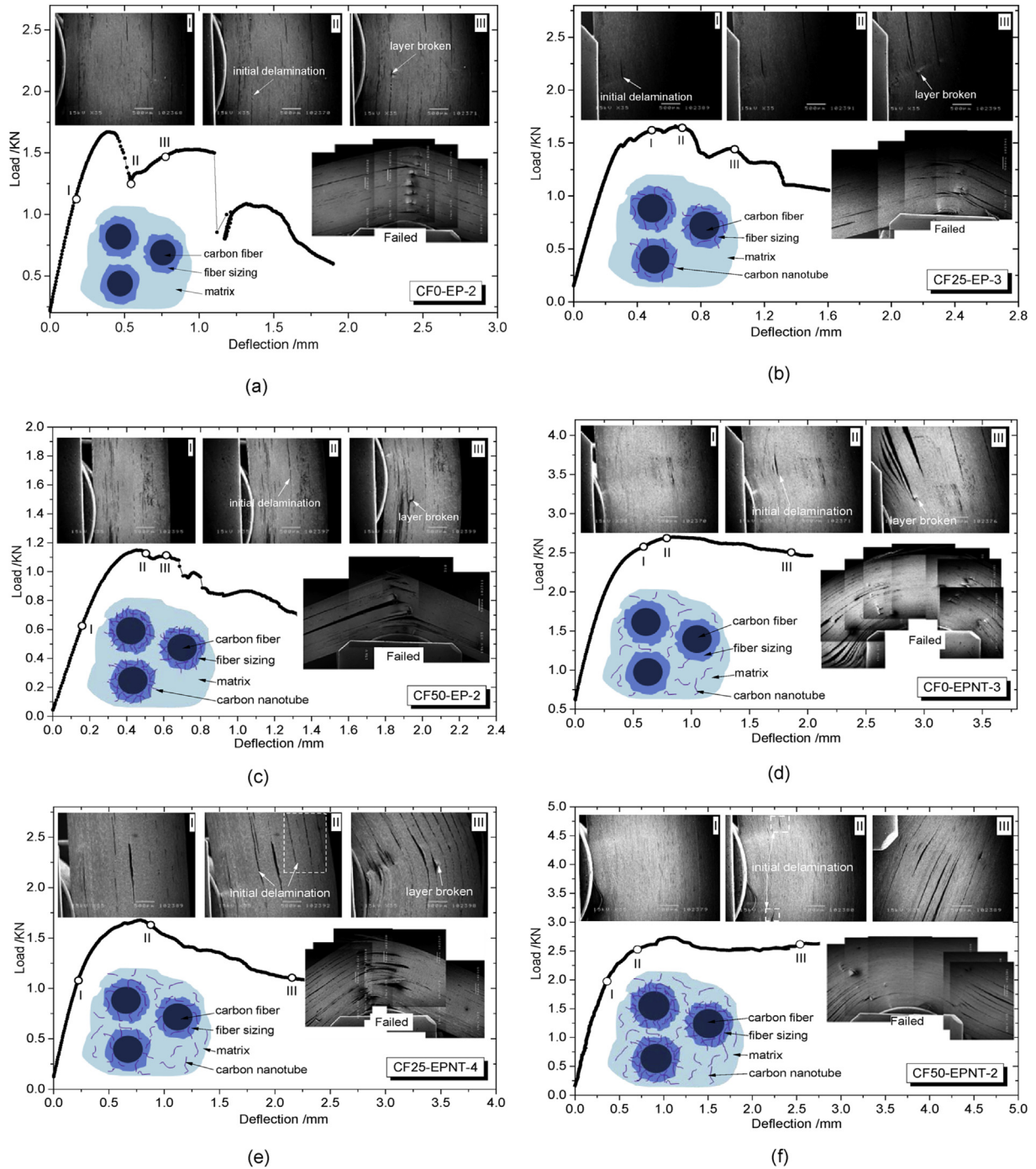


Fig. 5. Delaminating process of specimen (a) CF0-EP, (b) CF25-EP, (c) CF50-EP, (d) CF0-EPNT, (e) CF25-EPNT and (f) CF50-EPNT.

experimental data, and are in some cases up to 50% higher. The reason is (as mentioned above) that, instead of determining the input data by inverse modeling, we used the literature data for constituent properties. However, comparing the strengths (peak stresses) of the considered models, one can observe the following tendencies.

Adding the CNT in the polymer matrix increases the strength by 70 ... 77% (for CNT-free sizing and 50% CNTs in sizing). The introduction of 50% CNT in the fiber sizing leads to the 11% increase of strength (no CNT in matrix). The introduction of both 50% of CNT in sizing and CNT in the matrix leads to the 42% ... 88% increase of

strength (the higher the more the CNT content in the sizing) as compared with the CNT-free material. Comparing these data with the results of the section 0, we can see that the relations between results of simulations well correspond to some experimental results: 77% difference between composites with and without CNTs in matrix, and 42% ... 88% strength increase due to adding CNT both in fiber sizing and in matrix. The effect of adding CNT in the fiber sizing (keeping matrix CNT free) obtained in simulations is much lower than that that observed in the experiments (11% versus 36 ... 53%) (what hints on the possible other mechanisms, not included in our purely mechanical model).

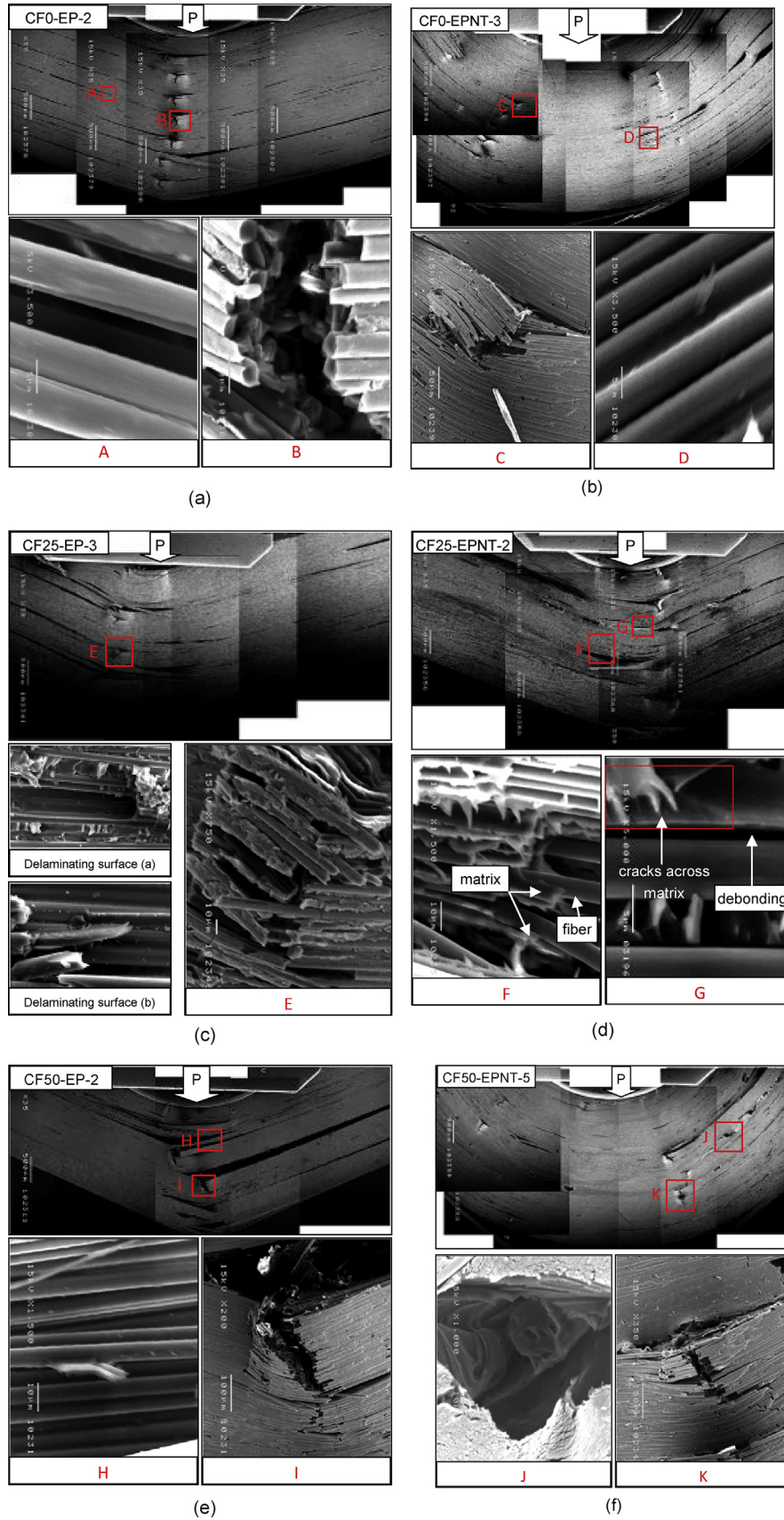


Fig. 6. Topography of delaminating cracks in specimen (a) CF0-EP, (b) CF0-EPNT, (c) CF25-EP, (d) CF25-EPNT, (e) CF50-EP and (f) CF50-EPNT.

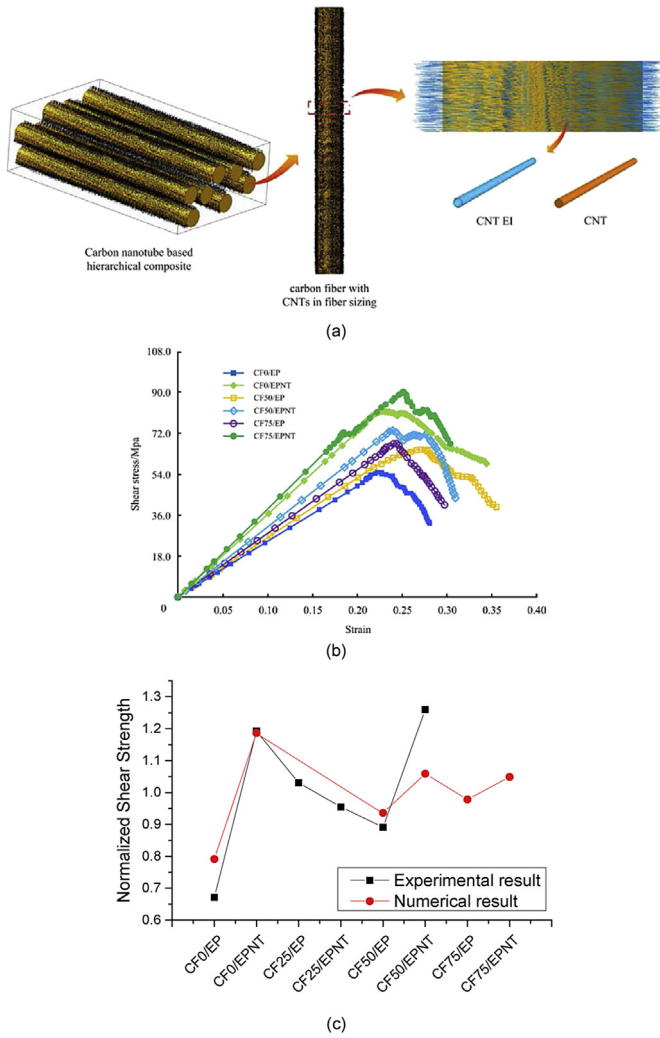


Fig. 7. Multiscale finite element model of the composite with 50% CNTs in sizing (a) and simulated stress–strain curves (b) and model–experiment comparison (c).

4.5. Discussion and comparison with literature data

In this section, we seek to compare the obtained theoretical and experimental results, as well as compare them with literature data.

Fig. 7c shows the curve of normalized shear strength for different structures obtained numerically and experimentally in the sections

Table 4
Materials and component properties.

Constituent	Elastic properties	Strength	Threshold and critical strain energy release rates
Polymer (epoxy) matrix	Young's modulus of 1.9 GPa, Poisson's ratio of 0.37	tensile strength of 68 MPa, compression strength of 88 MPa [39].	$G_{Ith} = 0.06 \text{ kJ/m}^2$ [46], $G_{Ic} = 0.173 \text{ kJ/m}^2$ [46], $G_{IIth} = 0.24 \text{ kJ/m}^2$, $G_{IIc} = 0.49 \text{ kJ/m}^2$ [46], $G_{IIIth} = 0.306 \text{ kJ/m}^2$, $G_{IIIc} = 0.49 \text{ kJ/m}^2$ [47,48]
Carbon fiber, radius 4 μm	Young's modulus 276 GPa, Poisson's ratio is 0.37 [40]	tensile and compressive strengths are 3000 MPa and 2800 MPa, respectively [39].	$G_{Ith} = 0.098 \text{ kJ/m}^2$ (Eq. (1) and [48]), $G_{Ic} = 0.636 \text{ kJ/m}^2$ (Eq. (1) and [47]), $G_{IIth} = 0.712 \text{ kJ/m}^2$ (Eq. (1) and [49]), $G_{IIc} = 3.744 \text{ kJ/m}^2$ (Eq. (1) and [49]), $G_{IIIth} = 1.598 \text{ kJ/m}^2$, $G_{IIIc} = 7.978 \text{ kJ/m}^2$
Carbon fiber/matrix interface; thickness 1.0 μm	$E_{C-M} = 27.79 \text{ GPa}$ [44]	tensile strength of 68 MPa	Carbon-matrix interface: $G_{Ith} = 0.079 \text{ kJ/m}^2$ [48], $G_{Ic} = 0.403 \text{ kJ/m}^2$ [47], $G_{IIth} = 0.476 \text{ kJ/m}^2$ [49], $G_{IIc} = 2.117 \text{ kJ/m}^2$ [49], $G_{IIIth} = 0.952 \text{ kJ/m}^2$, $G_{IIIc} = 4.234 \text{ kJ/m}^2$
Carbon nanotubes (CNT) radius 0.01 nm; length 0.8 μm CNT/matrix interface	Young's modulus of SWCNT 1 TPa; Poisson ratio is 0.2 [41] Young modulus 3.74 GPa, following the inverse analysis of graphene–epoxy interface [14]	tensile strength 30 GPa [42,43]	CNT–matrix interface: $G_{Ith} = 0.447 \text{ kJ/m}^2$ [44], $G_{IIc} = 1.93 \text{ kJ/m}^2$ [44]

3–4. The peak strength values were normalized by the average values over all cases. While the developed model is still very idealized (first of all, with view on the nanoscale structures), the simulated and experimental results do show close tendencies, and demonstrates qualitatively the correspondence between our numerical and experimental results. Further steps in this work will include the development of more detailed models, taking into account clustering, misalignment and non-ideal shapes of CNTs. The numbers obtained in the sections 3 and 4 are comparable with the estimations of the effect of CNTs on the composite properties given in Refs. [8–20]. It is of interest to compare our observations with the results of push-out test presented in Ref. [16]. The authors observed that the CNT additions (on matrix, on fibers or both) increased the peak forces in all cases, but the strongest effect (~3 times increase, 1.5 times or stronger than other cases) was for the CNT reinforcement on fibers with neat epoxy. Godara and colleagues observed that adding MWCNTs into fiber sizing improves the interfacial shear stress (IFSS), but the combination of CNTs on fiber sizing and in matrix was less effective, or even decrease the IFSS in the fiber push-out test. It is of interest that also in our cases, the average shearing strength is the highest for the composites with CNT around fibers, not in the matrix. The difference here is at the level of 21% (25% CNT) up to 81% (50% CNT in fiber coating). These numbers are very close to the numbers from Ref. [16]. The ILSS decrease tendency after adding 25% CNTs or more in fiber sizing and matrix is seen also in Fig. 7c.

It is of interest further to compare our observations with the results of the short beam shear experiment presented in Ref. [53]. Rahman et al. [53] dispersed amino-functionalized multiwall nanotubes (from 0 to 0.4 wt%) into the resin and also dispersed on the glass fiber surface. The highest ILSS is observed for the sample with 0.3 wt% CNTs [53]. TEM observations demonstrated that ILSS decreases with 0.4 wt% CNTs because of high surface area of nanotubes. This phenomenon also can be seen in our studies, after adding 25% CNTs into the fiber sizing.

According to [19,54–56], CNTs located in the interlaminar region increase ILSS by 2–45%, depending on the type, content and surface chemistry of CNTs. It is reasonable that the high content of CNTs in matrix may emerge into the interlaminar region thereby increasing the ILSS to some extent. Thus, relatively high content of CNTs in fiber sizing may reduce ILSS because of the high surface area while the CNTs in the matrix may increase the crack resistance in the interlaminar region.

Therefore both the experimental and numerical results in Fig. 7c undergo an increase tendency after the total content of CNTs in fiber sizing (which may disperse into interlaminar region) and matrix was relative high. The SEM picture on Fig. 6f also shows that

the delaminating area emerge in a thick matrix region (i.e., interlaminar region) subject to complex shearing.

All comparison analysis mentioned-above indicate that the experimental and numerical results in Sections 3 and 4 are reasonable. However, further steps related to the development of more detailed models, taking into account clustering, misalignment and non-ideal shapes of CNTs, are still necessary because of the complicated mechanism of influence of CNTs on the interlaminar shearing properties of carbon fiber composites.

5. Conclusion

In this work, the effect of the secondary CNT reinforcement, its distribution and content on the strength and fracture behavior of carbon fiber/polymer composites was studied both experimentally and numerically. The Short Beam Shearing tests had been carried out, with SEM observations of the damage evolution in the composites. In CFRP composites with virgin matrix and fiber sizing, the following damage mechanism was observed. The samples delaminated soon after they get into nonlinear stage in load-deflection curves. The delamination cracks dominate the interlaminar shear strength of this type of composites. The cracks propagate along the fibers interfaces in the direction along fiber axes. Then, delaminated layers subject to compression load broke which caused final failure of the whole materials.

Adding CNTs into the fiber sizing improves the fiber/matrix interface bonding. If the CNTs are added only to fiber sizing (and the matrix remains CNT-free), the delamination damage begins in the interface between fiber sizing and matrix, and is strongly influenced by the distribution and parameters of CNTs in the sizing.

CNTs in matrix improve the bonding capacity of fiber sizing and matrix, the material toughness and resistance to the delaminating crack propagation. Adding CNTs into the matrix leads to the long nonlinear stage on the load-deflection curves and ensures the high strength of the material. The addition of CNTs in the matrix (with virgin sizing) leads to the increase of ILSS by 77%. The addition of CNT in the fiber sizing (keeping matrix CNTs free) increases the toughness by 36%–53%. The addition of both CNTs in fiber sizing and in matrix leads to the increase in the ILSS by 42%–88%. Computational simulations led to similar estimations.

Summarizing, one can state that adding secondary CNTs nano-reinforcement into the matrix and sizing of carbon fiber/reinforced composites ensures strong increase of the composite strength. High volume content of CNTs in the sizing is better than lower content. The effect of secondary CNTs reinforcement is strongest when some small addition of CNTs in the polymer matrix is complemented by the fiber sizing with high content of CNTs.

Acknowledgment

The authors gratefully acknowledge the financial support of the Program of International S&T Cooperation (2010DFA64560), MOST (2010DFA64560) and the Danish Council for Strategic Research (DSF) via the collaborative project "High reliability of large wind turbines via computational micromechanics based enhancement of materials performances" (Ref. No. 10-094539) and the Danish Centre for Composite Structures and Materials for Wind Turbines (DCCSM) (Contract No. 09-067212) as well as the National Natural Science Foundation of China (11172318) and the 111 Project (B14006).

References

- Mishnaevsky Jr L, Brøndsted P, Nijssen R, Lekou DJ, Philippidis TP. Materials of large wind turbine blades: recent results in testing and modelling. *Wind Energy* 2012;15(1):83–97.
- Summerscales J, Short D. Carbon fibre and glass fibre hybrid reinforced plastics. *Composites* 1978;9(3):157–66.
- Sonparote PW, Lakkad SC. Mechanical properties of carbon/glass fibre reinforced hybrids. *Fibre Sci Technol* 1982;16(4):309–12.
- Manders PW, Bader MG. The strength of hybrid glass/carbon fibre composites. *J Mater Sci* 1981;16(8):2246–56.
- Mishnaevsky Jr L, Dai G. Hybrid and hierarchical polymer composites: computational modelling of structure-properties relationships. *Compos Struct* 2014;117:156–68.
- Mishnaevsky Jr L, Dai G. Hybrid carbon/glass fiber composites: micro-mechanical analysis of structure-damage resistance relationship. *Comput Mater Sci* 2014;81:630–40.
- Qian H, Greenhalgh ES, Shaffer MSP, Bismarck A. Carbon nanotube-based hierarchical composites: a review. *J Mater Chem* 2010;20:4751–62.
- Díez-Pascual AM, Naffakh M, Marco C, Gómez-Fatou MA, Ellis GJ. Multiscale fiber-reinforced thermoplastic composites incorporating carbon nanotubes: a review. *Curr Opin Solid State Mater Sci* 2014;18(2):62–80.
- Bekyarova E, Thostenson ET, Yu A, Itkis ME, Fakhrutdinov D, Chou T, et al. Functionalized single-walled carbon nanotubes for carbon fiber-epoxy composites. *J Phys Chem C* 2007;111:17865–71.
- Bekyarova E, Thostenson ET, Yu A, Kim H, Gao J, Tang J, et al. Multiscale carbon nanotube-carbon fiber reinforcement for advanced epoxy composites. *Langmuir* 2007;23:3970–4.
- Wicks SS, de Villoria RG, Wardle BL. Interlaminar and intralaminar reinforcement of composite laminates with aligned carbon nanotubes. *Compos Sci Technol* 2010;70(1):20–8.
- Storck S, Malecki H, Shah T, Zupan M. Improvements in interlaminar strength: a carbon nanotube approach. *Compos Part B* 2011;42:1508–16.
- Warrier A, Godara A, Rochez O, Mezzo L, Luizi F, Gorbatiikh L, et al. The effect of adding carbon nanotubes to glass/epoxy composites in the fibre sizing and/or the matrix. *Compos Part A* 2010;41(4):532–8.
- De Greef N, Gorbatiikh L, Godara A, Mezzo L, Lomov SV, Verpoest I. The effect of carbon nanotubes on the damage development of carbon fiber/epoxy composites. *Carbon* 2011;49(14):4650–64.
- Godara A, Mezzo L, Luizi F, Warrier A, Lomov SV, van Vuure A, et al. Influence of carbon nanotube reinforcement on the processing and the mechanical behaviour of carbon fiber/epoxy composites. *Carbon* 2009;47(12):2914–23.
- Godara A, Gorbatiikh L, Kalinka G, Warrier A, Rochez O, Mezzo, et al. Interfacial shear strength of a glass fiber/epoxy bonding in composites modified with carbon nanotubes. *Compos Sci Technol* 2010;70(9):1346–52.
- Zhou Y, Pervin F, Rangari VK, Jeelani S. Fabrication and evaluation of carbon nanofiber filled carbon/epoxy composite. *Mater Sci Eng A* 2006;426:221–8.
- Zhu J, Khabashesku V, Imam A, Crane R, Lozano K, Barrera E. Processing and properties of polymer composites reinforced by functionalized SWNTs. In: 5th Pacific rim int conf advanced materials and processing, vol. 475–479; 2005. p. 1059–62.
- Zhu J, Imam A, Crane R, Lozano K, Khabashesku V, Barrera EV. Processing a glass fiber reinforced vinyl ester composite with nanotube enhancement of interlaminar shear strength. *Compos Sci Technol* 2007;67(7–8):1509–17.
- Gojny FH, Wichmann MHG, Fiedler B, Schulte K. Influence of different carbon nanotubes on the mechanical properties of epoxy matrix composites—a comparative study. *Compos Sci Technol* 2005;65:2300–13.
- ASTM standard D2344/D2344M. Standard test method for short-beam strength of polymer matrix composite materials and their laminates. West Conshohocken, PA: ASTM International; 2000. http://dx.doi.org/10.1520/D2344_D2344M. www.astm.org.
- Zhou HW, Yi HY, Gui LL, Dai GM, Peng RD, Wang HW, et al. Compressive damage mechanism of GFRP composites under off-axis loading: experimental and numerical investigations. *Compos Part B* 2013;55:119–27.
- Mishnaevsky Jr L, Zhou HW, Yi HY, Gui LL, Peng RD, Wang HW. Microscale damage mechanisms and degradation of fiber-reinforced composites for wind energy applications: results of Danish-Chinese collaborative investigations. *J Compos Mater* 2014;48(24):2977–91.
- Zhou HW, Mishnaevsky Jr L, Brøndsted P, Tan J, Gui L. SEM insitu laboratory investigations on damage growth in GFRP composite under three-point bending tests. *Chin Sci Bull* 2010;55(12):1199–208.
- Dai GM, Mishnaevsky Jr L. Fatigue of multiscale composites with secondary nanoplatelet reinforcement: 3D computational analysis. *Compos Sci Technol* 2014;91:71–81.
- Mishnaevsky Jr L. Nanostructured interfaces for enhancing mechanical properties of materials: computational micromechanical studies. *Compos Part B* 2015;68:75–84.
- Dai GM, Mishnaevsky Jr L. Damage evolution in nanoclay-reinforced polymers: a three-dimensional computational study. *Compos Sci Technol* 2013;74:67–77.
- Mishnaevsky Jr L, Brøndsted P. Three-dimensional numerical modelling of damage initiation in UD fiber-reinforced composites with ductile matrix. *Mater Sci Eng A* 2008;498(1–2):81–6.
- Dai GM, Mishnaevsky Jr L. Graphene monolayer nanocomposites: 3D simulation of damage and fracture. *Comput Mater Sci* 2014;95:684–92.
- Peng RD, Zhou HW, Wang HW, Mishnaevsky Jr L. Modeling of nano-reinforced polymer composites: microstructure effect on the Young's modulus. *Comput Mater Sci* 2012;60:19–31.

- [31] Wang HW, Zhou HW, Peng RD, Mishnaevsky Jr L. Nanoreinforced polymer composites: 3D FEM modeling with effective interface concept. *Compos Sci Technol* 2011;71(7):980–8.
- [32] Wang HW, Zhou HW, Peng RD, Mishnaevsky Jr L. Single fibre and multifibre unit cell analysis of strength and cracking of unidirectional composites. *Comput Mater Sci* 2009;46:810–20.
- [33] Greco F, Leonetti L, Blasi PN. Non-linear macroscopic response of fiber-reinforced composite materials due to initiation and propagation of interface cracks. *Eng Fract Mech* 2012;80:92–113.
- [34] Goyal VK, Johnson ER, Davilia CG. Irreversible constitutive law for modeling the delamination process using interfacial surface discontinuities. *Compos Struct* 2004;65:289–305.
- [35] Rybicki EF, Kanninen MF. A finite element calculation of stress intensity factors by a modified crack closure integral. *Eng Fract Mech* 1977;9:931–8.
- [36] Krueger R. Virtual crack closure technique: history, approach and applications. *Appl Mech Rev* 2004;57:109–43.
- [37] Belytschko T, Gracie R, Ventura G. A review of extended/generalized finite element methods for material modeling. *Modell Simul Mater Sci Eng* 2009;17: 1–24.
- [38] Sukumar N, Moes N, Moran B, Belytschko T. Extended finite element method for three-dimensional crack modeling. *Int J Numer Meth Eng* 2000;48: 1549–70.
- [39] Dai GM, Mishnaevsky Jr L. Fatigue of hybrid carbon/glass composites: 3D computational modelling. *Compos Sci Technol* 2014;94:71–9.
- [40] Mishnaevsky Jr L, Brøndsted P. Statistical modelling of compression and fatigue damage of unidirectional fiber reinforced composites. *Compos Sci Technol* 2009;69(3–4):477–84.
- [41] Sanche-Portal D, Artacho E, Soler JM, Rubio A, Ordejon P. Ab-initio structural, elastic, and vibrational properties of carbon nanotubes. *Phys Rev B* 1999;59: 12678–88.
- [42] Yu MF, Files BS, Arepalli S, Ruoff RS. Tensile loading of ropes of single wall carbon nanotubes and their mechanical properties. *Phys Rev Lett* 2000;84: 5552–5.
- [43] Yu MF, Lourie O, Dyer MJ, Moloni K, Kelly TF, Ruoff RS. Strength and breaking mechanism of multiwalled carbon nanotubes under tensile load. *Science* 2000;287:637–40.
- [44] Dai GM, Mishnaevsky Jr L. Carbon nanotube reinforced hybrid composites: computational modelling of environmental fatigue and their usability for wind blades. *Compos Part B* 2015;78:349–60.
- [45] Pinho ST, Robinson P, Lannucci L. Fracture toughness of the tensile and compressive fibre failure modes in laminated composites. *Compos Sci Technol* 2006;66:2069–79.
- [46] Reeder JR. 3D mixed-mode delamination fracture criteria—an experimentalist's perspective. NASA Langley Research Center, M/S 188E, Hampton VA 23681-2199, USA.
- [47] Schwartz HS, Hartness JT. Effect of fiber coatings on interlaminar fracture toughness of composites. In: *Toughened composites: symposium on toughened composites*; 1987. 937. Baltimore, MD.
- [48] Singh S, Greenhalgh E. Delamination growth in epoxy-matrix composites under cyclic loading: implications for design and certification. In: *8th Europ conf composite materials (ECCM-8)*, Naples, Italy; June, 1998.
- [49] O'Brien TK, Johnston WM, Toland GJ. Mode II interlaminar fracture toughness and fatigue characterization of a graphite epoxy composite material. NASA Langley Research Center, NASA/TM-2010-216838, Hampton, VA 23681-2199, USA.
- [50] Wichmann MHG, Sumfleth J, Gojny FH, Quaresimin M, Fiedler B, Schulte K. Glass-fibre-reinforced composites with enhanced mechanical and electrical properties e benefits and limitations of a nanoparticle modified matrix. *Eng Fract Mech* 2006;73:2346–59.
- [51] Zhang QH, Liu JW, Sager R, Dai L, Baur J. Hierarchical composites of carbon nanotubes on carbon fiber: influence of growth condition on fiber tensile properties. *Compos Sci Technol* 2009;69:594–601.
- [52] Sager RJ, Klein PJ, Lagoudas DC, Zhang Q, Liu JW, Dai L, et al. Effect of carbon nanotubes on the interfacial shear strength of T650 carbon fiber in an epoxy matrix. *Compos Sci Technol* 2009;69:898–904.
- [53] Rahman MM, Zainuddin S, Hosur MV, Robertson CJ, Kumar A, Trovillion J, et al. Effect of NH₂-MWCNTs on crosslink density of epoxy matrix and ILS properties of e-glass/epoxy composites. *Compos Struct* 2013;95: 213–21.
- [54] Hsiao KT, Alms J, Advani SG. Use of epoxy/multiwalled carbon nanotubes as adhesives to join graphite fibre reinforced polymer composites. *Nanotechnology* 2003;14:791–3.
- [55] Thakre PR, Lagoudas DC, Zhu J, Barrera EV, Gates TS. Processing and characterization of epoxy/SWCNT/woven fabric composites. In: *Proceedings of 47th AIAA Structure, Structural Dynamics, and Materials Conference*, Newport, RI, May 1–4, 2006. AIAA; 2006. p. 1857.
- [56] Qian H, Greenhalgh ES, Shaffer MSP, Bismarck A. Carbon nanotube-based hierarchical composites: a review. *J Mater Chem* 2010;20(23):4729–956.